JOURNAL OF GEOPHYSICAL RESEARCH, VOL. 101, NO. C10, PAGES 22,631–22,645, OCTOBER 15, 1996

Statistical analysis of the surface circulation of the California Current

Mark S. Swenson
Atlantic Oceanographic and Meteorological Laboratory, NOAA, Miami, Florida

Pearn P. Niiler
Scripps Institution of Oceanography, University of California, San Diego, La Jolla

Abstract. We use a set of mixed-layer drifting buoy trajectories from the California Current (20°N–40°N) during 1985–1990 to obtain statistically reliable estimates of the mean currents, the mean variance field, and the geographically varying diffusivity, integral timescales, and integral space scales. Typical values for the diffusivity are $1.1–8.7 \times 10^7$ cm^2 s^{-1}, while the timescales and space scales are 2.1–7.1 days and 16–59 km, respectively. The variance field displays a strong westward gradient out to 125°W, and diffusivity shows a tendency to decrease toward the southwest part of the domain. Significant anisotropy is found in the variance field near the coastal boundary and at 30°N, 130°W, which is the region where the subarctic and northern subtropical fronts approach the California Current. The antisymmetric component of the diffusivity tensor indicates that cyclonic eddies dominate the mesoscale signature of drifters in this region. We seek simple parameterizations to relate the scales of motion of the random velocity field to the diffusivity by testing least squares fits to $\kappa^\infty \propto u_0^2 T$ and $\kappa^\infty \propto u_0 L$, where u_0^2 is the velocity variance. We found no cases for which these two hypotheses could be distinguished. For the meridional component the linear regressions are not successful, which suggests that the meridional departure velocities result from a flow regime that is significantly organized by, for example, waves or coherent structures. A subset of the drifters measured temperature along their tracks, and we use the resultant data to produce the first direct estimates of the horizontal eddy heat flux divergence based on Lagrangian estimates. In addition, we separately compute the "eddy diffusivity" parameterization of the eddy heat flux divergence, $\nabla \cdot \langle \mathbf{u}'\theta' \rangle = \nabla(\kappa \nabla \Theta)$, using our diffusivity estimates and a sea surface temperature climatology. The two independent terms agree well, which provides a measure of reassurance about the diffusivity estimates. The eddy heat flux divergence in the California Current is very small (<5 W m^{-2}) and does not appear to be significant in the long-term heat budget of the upper ocean in this region.

1. Introduction

The prevailing winds off California are equatorward throughout the year, and the resultant offshore Ekman transport induces upwelling along the coast [*Wooster and Reid*, 1963]. The California Current is, consequently, a nutrient-rich system that sustains a highly productive food web [*Walsh*, 1977]. The Coastal Transition Zone Experiment helped establish that the offshore supply of nutrients also depends on a complex pattern of cross-shelf circulation that involves the formation of offshore-directed jets and eddies [*Strub et al.*, 1991]. The origin of the eddies and jets remains uncertain but may include the effects of topography and coastal variations, variations in wind forcing, and baroclinic instability processes. Although a variety of models have produced simulations that resemble the circulation of the California Current, models that produce reasonable variability are sensitive to the basic flow state, details of the topographic variations, and/or subgridscale parameterizations [*McCreary et al.*, 1991; *Allen et al.*, 1991; *Haidvogel et al.*, 1991]. It is therefore critical that the performance of models be evaluated against observations. In this paper, we use the drifting-buoy database to determine the mean advective and eddy diffusive transports in the mixed layer of the California Current between 20°N and 40°N during 1985–1990.

This study builds on the results of *Poulain and Niiler* [1989] and *Brink et al.* [1991], each of which analyzed a subset of the data analyzed herein. The full data set is substantially larger, which affords greater statistical reliability and enables us to make estimates of the geographical variations of the velocity field, the variance field, the diffusivity, and the decorrelation timescales and space scales along with error estimates. In addition, we use the subset of these drifters equipped with thermistors to explore for the first time the joint velocity-temperature statistics of the California Current from a Lagrangian perspective.

The easiest description of the basic transport processes in a flow is in the Lagrangian reference frame; in particular, it is necessary to adopt a Lagrangian perspective to describe the effects of eddy variability on mean transport [*Davis*, 1991a]. Quasi-Lagrangian drifting buoys accurately measure lateral ve-

Paper number 96JC02008.
0148-0227/96/96JC-02008$09.00

locity [*Niiler et al.*, 1987, 1995] and inherently average over space and time, so they are well suited for measuring the large-scale, low-frequency field that produces the mean lateral transport [*Davis*, 1985, 1991a]. (The buoys are "quasi-Lagrangian" because they are constrained to stay at a constant depth and therefore do not follow vertical motions.) A number of regional studies of the upper ocean circulation [*Richardson*, 1983; *Davis*, 1985; *Poulain and Niiler*, 1989; *Brink et al.*, 1991] have been based on drifting-buoy observations. In one way or another each of these studies faced the problem of reconciling the velocity observations within a framework of a model of advection and eddy transport.

The challenge is to select a scale separation that allows one to parameterize the effect of the small-scale, unresolved motions in terms of the resolved scales to obtain a closed formulation of the resolved scales. This is the "eddy diffusivity" analogy with molecular transport. If we denote the concentration of a passive tracer by Θ and ensemble averages by $\langle\ \rangle$, the conventional framework for development involves the separation $\Theta = \langle\theta\rangle$, $\theta' = \theta - \Theta$, $\mathbf{U} = \langle\mathbf{u}\rangle$, and $\mathbf{u}' = \mathbf{u} - \mathbf{U}$ in terms of which Θ evolves as

$$\partial_t\Theta + \mathbf{U}\cdot\nabla\Theta = Q - \nabla\cdot\mathbf{E} \tag{1}$$

where

$$Q(\mathbf{x}, t) = \langle q(\mathbf{x}, t)\rangle, \qquad \mathbf{E}(\mathbf{x}, t) = \langle\mathbf{u}'(\mathbf{x}, t)\theta'(\mathbf{x}, t)\rangle,$$

q is the source of θ, and $\mathbf{E}$ is what we seek to relate to mean properties. Usually, one asserts an analogy between eddies and molecules to invoke a flux versus mean gradient law, which yields $\nabla\cdot\mathbf{E} = \nabla(\kappa\nabla\Theta)$, where κ is a constant or slowly varying eddy diffusivity. The circumstances under which this is a useful oceanographic approximation have been a subject of debate [*Holloway*, 1989], but (1) with κ = constant is used in most practical applications because it is conceptually simple and easy to implement. It is strictly valid, however, only for stationary and homogenous statistics in the limit of infinitesimal eddies. Such considerations led *Davis* [1987] to propose a generalized advection-diffusion model that is valid when the scales of the eddies are small but not infinitesimal and for which the homogeneity condition is relaxed. Practical use of this model is facilitated by *Davis* [1991a], who provides an evaluation of the methods for using trajectories of current-following drifters to determine advective and eddy transports in the ocean. This theoretical framework is important for at least three reasons. First, it provides a conceptual framework based on rational approximations that allows the analyst to evaluate systematically the degree to which the assumptions of the theory are met. Second, it provides explicit formulae for sampling errors. In particular, it shows that estimates of the sampling error for diffusivity grow with time like $t^{1/2}$. This is a basic result which would hold even if the number of observations of $\kappa(t)$ did not decrease as t increases. Historically, this has made measurements of diffusivity uncertain because $\kappa(t)$, which has been obtained as the integral of the velocity covariance, often does not appear to approach a constant for large t. This has led investigators to compute diffusivities by integrating estimates of the covariance over shorter times for which they believed the true covariance had reached a value of zero. The methods for determining the shorter times over which to integrate have been ad hoc because a formal evaluation of covariance uncertainties can only be expressed as a complicated convolution integral [*Flierl and McWilliams*, 1977]. Finally, it provides a prescription for practical calculations of diffusivity that minimizes sampling errors. In this paper we use *Davis*'s [1991a] approach to calculate estimates of the upper ocean transports using a set of mixed-layer drifting-buoy trajectories from the California Current during 1985–1990.

We organize the paper as follows. In section 2 we discuss the data set and our processing procedures. Section 3 describes our methodology and presents the circulation statistics for the California Current, and section 4 provides a discussion and review.

2. Data Set

2.1. Overview

We obtained the data for this study from five experiments that deployed satellite-tracked drifting buoys in the California Current system during late spring to early fall during 1985–1988 (Figure 1 and Table 1). The drifters, which were drogued to 15-m depth, are calibrated, and expected slips are <2 cm s^{-1} for the conditions expected to be encountered [*Niiler et al.*, 1987; *Mackas et al.*, 1989; *Niiler et al.*, 1995]. In 1985 and 1986, 29 buoys were deployed and tracked for up to 13 months. Although these drifters had a thermistor mounted in the surface float, they did not yield oceanographically useful temperature records because they were inadequately insulated from the diurnal heating of the float itself. The position data from these instruments have been analyzed extensively [*Niiler et al.*, 1989; *Poulain*, 1990], including a statistical analysis [*Poulain and Niiler*, 1989]. In 1987, 25 drifters were deployed during the first year of the Coastal Transition Zone Experiment (CTZ) [*Brink and Cowles*, 1991]. These were equipped with thermistors on the tether line at depths of 0, 12, and 18 m, although only the middle thermistor gave consistently good results. These instruments had survivability problems, and none lasted longer than 3 months [*Paduan and Niiler*, 1990]. Drifting buoys were deployed during two independent experiments in 1988. Fifty instruments were deployed in the coastal water near Point Arena as part of CTZ [*Swenson et al.*, 1992; *Brink et al.*, 1991], and 21 were deployed farther south as part of the Fronts 88 Cruise [*Venrick et al.*, 1991]. The former were equipped with four thermistors at depths of 0, 3.5, 11.8, and 17.4 m, while the latter had a thermistor mounted in the surface float. Both of these experiments had buoys that transmitted useful data for up to 20 months, although the thermistors failed somewhat earlier. For the instruments deployed in 1988 the transmitters were programmed to transmit on a 2-and-1 duty cycle (2 days off and 1 day on) after an initial 90-day period of continuous transmissions. *Brink et al.* [1991] have published a statistical analysis of the CTZ position data prior to 1989.

2.2. Processing

In processing the positions we attempted to account for and remove the high-frequency inertial-band wave energy [*Poulain*, 1990] to avoid aliasing the energy into the low-frequency motions that are the primary interest of our study. More mature reflection indicates that this was superfluous. The inertial-band energy is at least 1 order of magnitude less than the low-frequency motions, and the processing scheme did not yield results significantly different than those obtained by simple daily averaging. The effect of the fitting procedure used was to filter out velocity variance for periods under 5 days.

In processing the temperatures we attempted to account for and remove the high-frequency diurnal variations in a manner similar to that of position data. For similar reasons this was

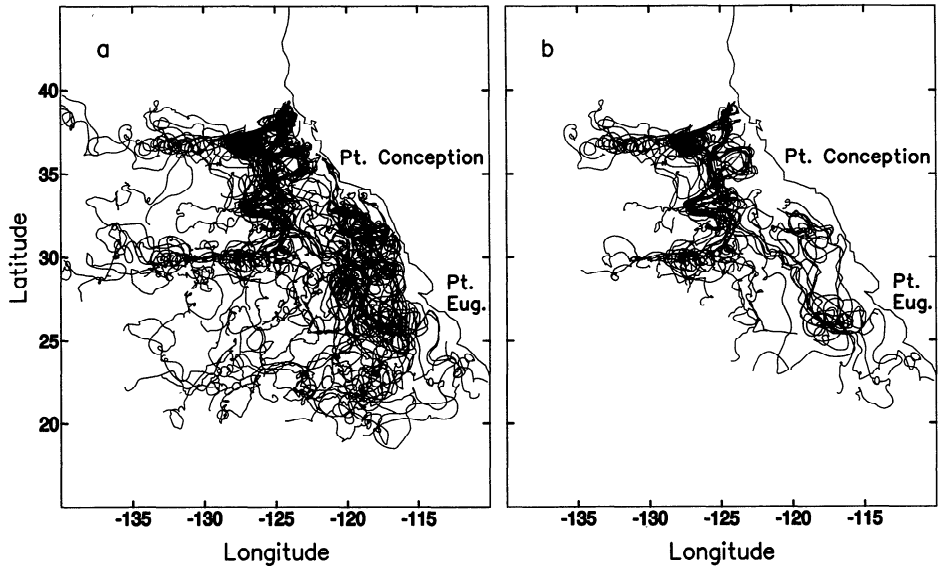

Figure 1. (a) Summary plot of 124 free-drifting buoy trajectories, 1985–1990. (b) Summary plot of free-drifting buoy trajectories used in the analysis of the joint velocity-temperature statistics.

also superfluous, and the results are not significantly different from those obtained by simple daily averaging. The interpretation of the temperature records is difficult because the drifter design changed from experiment to experiment as we learned the best way to incorporate the temperature sensors. The results were spotty, so that absolute values of the temperatures cannot be meaningfully compared between drifters. The time change of the temperature, however, is well determined, and we use the data in this form.

2.3. Data Distribution

Including the 2-and-1 duty cycle data, we have a total of 24,470 buoy days of data. The data are bounded by 141°W–109°W and 18°N–40°N. The first fix is on July 8, 1985, and the last is on June 5, 1990, so the observations span 1793 days. The range in kilometers meridionally is ~2450 km, whereas the range zonally is ~3000 km. We summarize the distribution of data with time in Figure 2. We see that nearly three quarters of the data are obtained during late summer to early winter.

Although the CTZ deployments in 1987 were equipped with thermistors, none of them worked for more than 2 months.

Table 1. Summary of the Basic Characteristics of the Data Obtained From Each Experiment

Experiment	Buoys	Transmission Schedule	Fixes	Days	Fixes/Day	Useful Temperatures?*
FRONTS85	20	continuous	23,201	4,624	5.0	no
FRONTS86	9	continuous	8,188	1,304	6.3	no
CTZ87	25	continuous	4,517	780	5.8	no
CTZ88	50	continuous	24,613	3,310	7.4	yes
	39	2-and-1	28,933	12,688	2.3	yes
FRONTS88	20	continuous	6,763	1,140	5.9	yes
	11	2-and-1	1,037	678	1.5	yes
Total	124	continuous	67,282	11,158	6.0	
	50	2-and-1	29,970	13,366	2.2	
Grand total	124		97,252	24,252	4.0	

*Indicates whether the experiment yielded good temperature records longer than 90-days duration.

The portion of the data set which recorded useful temperature measurements (here regarded as 3 months or longer records) is derived entirely from the 1988 deployments and consists of 9900 buoy days of data (Figure 2). The seasonal distribution of this subset closely parallels that of the full data set. The geographical distribution of the tracks during times when useful temperature measurements were obtained is depicted in Figure 1b.

2.4. Drifter Tracks

Although the tracks of the full data set (Figure 1a) present a tangled and confusing picture, there are several prominent features worthy of notice. The northern part of the domain is dominated by the deployments from CTZ88, nearly all of which sampled a narrow high-speed offshore jet that extended from ~124°W, 38°N to ~128°W, 37°N [*Swenson et al.*, 1992]. A large cyclonic eddy marks the end of the offshore extent of the filament at 127.5°W, 37°N. This feature dominated the local flow pattern and was very stable; drifters circulated within the eddy for more than 60 days. Extending farther seaward are tracks from drifters trapped in a cyclonic eddy that propagated nearly due west along 37°N out to nearly 135°W. Centered at ~36°N, 124°W is an "S"-shaped pattern lying entirely north of 34.5°N that was mapped out in the same location in both 1987 and 1988, which suggests a seasonally recurring cyclonic-anticyclonic eddy pair. South of the offshore jet extending from 36°N to 30°N between 123°W and 127°W is a meandering pattern of generally southward flow that ends at 30°N, where the drifters move westward as far as 140°W. The features of the southern part of the domain are not as dramatic, but there is clear evidence of a recurring large cyclonic eddy northwest of Punta Eugenia at 28°N, 120°W. There is also a strong tendency for the motions to go westward as the drifters reach ~22°N.

3. Statistics

We expect the near-surface velocity field of the California Current to exhibit significant nonstationarity and inhomogeneity [*Poulain and Niiler*, 1989; *Brink et al.*, 1991], but nonstationarity cannot be adequately explored with the present data set.

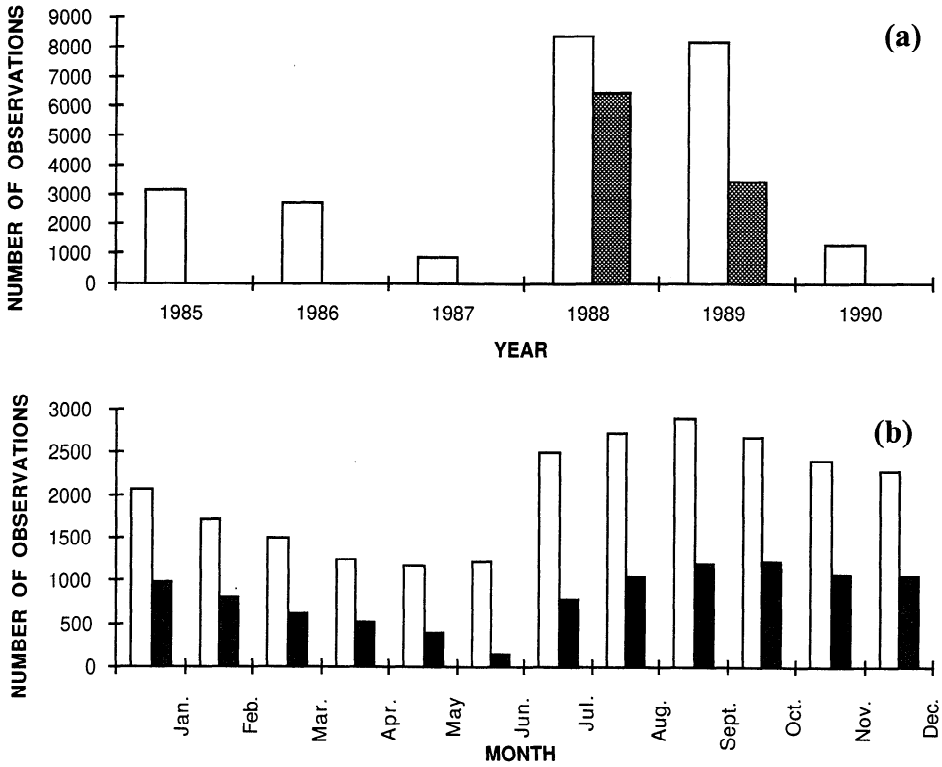

Figure 2. Frequency distribution of the number of daily drifting-buoy velocity observations as a function of (a) year and (b) month. Open bars represent the full data set, and solid bars represent the portion with useful temperatures.

Furthermore, the sampling is not adequate to resolve interannual variations. Although the ocean produces a seasonal signal in the velocity statistics as well as in the temperature statistics, the majority (75%) of measurements are from the summer and fall (Figure 2b), so that our analysis is representative of that time of year. The drifters were all deployed in late spring to early fall in two localized regions. As the mean southward flow carried the drifters southward, they sampled the flow at progressively later times, so that our analysis aliases seasonal variability into the spatial variability that we explicitly identify and discuss. Given the data set, there is no way to mitigate this unfortunate circumstance; we must simply keep it in mind during the analysis. Nonetheless, the spatial variability of the velocity statistics is an important part of the description of the general circulation of the California Current.

The way we choose to present such a description depends on the conceptual model of oceanic transport that we choose. Drifters are "moving current meters," but because the basic transport processes by which eddy variability modifies mean transport are most naturally described in a Lagrangian framework, drifter observations are more valuable than as just velocimeters. *Davis* [1987, 1991a] advanced a generalized advection-diffusion model to exploit the power of Lagrangian statistics to describe the effects of eddy variability on mean transport. This model provides the conceptual underpinning of our study. It provides an Eulerian representation of material particle dispersion that relaxes the requirement of flux-gradient models that property fluxes supported by velocity variability must be determined locally. This theory defines diffusivity as an observable Lagrangian velocity statistic that is a generalization of the single-particle diffusivity of *Taylor* [1921] to circumstances with mean flow. Similarly, the eddy flux, which is partially specified in terms of the recent history of the mean concentration field, reduces to the familiar eddy-diffusivity formulation for times long compared with the decorrelation time of Lagrangian velocity variability. The model's utility for this study is that it provides a rational framework for (1) mapping mean velocity and diffusivity, (2) estimating sampling errors and biases, and (3) interpreting the transport in regions where $\kappa(t)$ does not approach an asymptotic value, κ^{∞}, in a short time, that is, where eddy diffusivity is problematical.

3.1. Displacement Statistics

The restrictions under which *Davis*'s [1987] theory is valid are much less stringent if the velocity departure probability density is approximately Gaussian. If the velocity departures are Gaussian, the only scale restriction is that predictable displacements be smaller than the inhomogeneity scale, where the predictable displacements are those derived from a statistically optimized model for predicting a particle's trajectory from knowledge of its position $\mathbf{x}$ at time t and of its velocity at that time. This roughly corresponds to the requirement that the Lagrangian length scale be small compared to the distance over which the mean velocity and eddy kinetic energy vary significantly. Furthermore, the Gaussian-$\mathbf{u}$ condition avoids the requirement that the scale of the initial condition and source distribution of Θ be large. To what extent are the velocity departure statistics in the California Current Gaussian? To explore this question, we create composite time series of departure velocities relative to the local mean and normalized by the local variance. Local mean and variance are the estimates of mean and variance obtained by pooling all observations in bins $2° \times 2°$ or $5° \times 5°$. We compare these time series to the Gaussian distribution by means of the Kolmogorov-

Smirnov Test [*Press et al.*, 1992] modified to account for the correlation found in the time series. That is, we use for the degrees of freedom the length of the time series divided by 2 times the typical integral timescale [*Riser and Rossby*, 1983], which we conservatively take as 5 days (see Tables 6 and 7). Figure 3 shows the histograms for the zonal and meridional velocity departures for four different cases. For each of the resolutions, 2° × 2° and 5° × 5°, we consider two cases: (1) all of the data and (2) only data that are south of 35°N and westward of a diagonal that runs from 40°N, 130°W to 20°N, 110°W, which we refer to as "offshore." In the upper corner of each panel we include the probability that the Kolmogorov-Smirnov statistic would by chance be at least as large as that observed. Small probability ($\alpha \ll 1$) corresponds to cases where the time series is significantly different (at the $1 - \alpha$ confidence level) from Gaussian. We see that the zonal velocity departures are not significantly different from Gaussian at the 95% confidence level for any of the cases considered and the zonal velocity departures are always more nearly Gaussian than the meridional ones. For both velocity components, departures are more nearly Gaussian for the offshore case compared to the full data set. Departures calculated using the 2° × 2° resolution mean and variance fields are more nearly Gaussian than those calculated using the 5° × 5° fields, which indicates that errors in accounting for the spatial variations of the mean fields tend to move the departure statistics away from Gaussianity. The coast and the region north of 35°N tend to introduce non-Gaussianity in the velocity departure statistics to the extent that the meridional velocity departures are significantly different from Gaussian at the 95% confidence level for the full data set. These results indicate that *Davis*'s [1987] theory is applicable to the velocity departure statistics of the zonal component over the entire domain and for the meridional component in the offshore region. Results for the meridional component near the coast and north of 35°N must be viewed with caution.

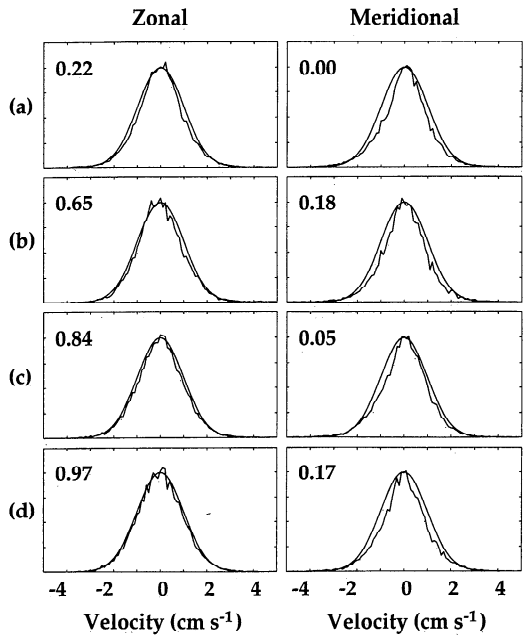

Figure 3. Histograms of velocity departure statistics for the zonal and meridional components for (a) 5° × 5° resolution and all data, (b) 5° × 5° resolution and "offshore" data, (c) 2° × 2° resolution and all data, and (d) 2° × 2° resolution and offshore data. Offshore data refer to the region south of 35°N and westward of a line that runs from 40°N, 130°W to 20°N, 110°W. The number in the upper left-hand corner of each figure part is the probability that the Kolmogorov-Smirnov statistic would be at least as large as that observed by chance. Small values correspond to cases where the sample distribution is significantly different from Gaussian. Values >0.05 indicate that the null hypothesis is rejected at the 95% confidence level.

3.1.1. Full data set. We first calculate the flow statistics without accounting for spatial variability of the flow. This calculation relies on the assumption that the mean flow can be meaningfully characterized by a single velocity. Given our knowledge of the flow structure in the California Current [*Poulain and Niiler*, 1989; *Brink et al.*, 1991], this assumption is suspect. It is useful, however, because it provides a basic overview or summary of the statistics and reveals some robust insights about the variability and because inadequacies in the analysis provide guidelines for refinements. The overall mean velocity, based on 24,470 daily samples, is $\mathbf{U} = (-0.41, -3.95)$ cm s^{-1}. Variances about the mean are $\langle u'u' \rangle = 160$, $\langle v'v' \rangle = 141$, and $\langle u'v' \rangle = 11$ cm^2 s^{-2}, the first two of which correspond to root mean square speeds of (13, 12) cm s^{-1}. These values are similar to those found by *Poulain and Niiler* [1989], who obtained $\mathbf{U} = (0.3, -3.8)$ cm s^{-1}, $\langle u'u' \rangle = 103$, and $\langle v'v' \rangle = 119$ cm^2 s^{-2}. A principal axes decomposition yields a major (minor) axis with variance of 164 (136) cm^2 s^{-2} with the major axis aligned along $\theta = 24°$, where $\theta = 0°$ is due east. This is significantly anisotropic at the 95% confidence level based on the conservative assumption that the Lagrangian timescale is 5 days (see Tables 6 and 7). The major axis is roughly aligned with the offshore jet in the northern part of the domain, which suggests that this jet introduces the dominant anisotropic feature. This is confirmed by a calculation that includes only data south of 35°N, which yields lower variances and a major axis aligned along $\theta = -21°$ that is oblique to the offshore jet. From such a broad perspective we cannot estimate an array bias, which depends on estimates of $\nabla(\ln C)$ and $\nabla \mathbf{U}$, where $C(\mathbf{x})$ is the mean concentration of floats averaged over the time interval of interest [*Davis*, 1991a].

As discussed above, the maximum slip expected under the conditions encountered in the California Current is <2 cm s^{-1}. The slip is directed along the prevailing winds, which are predominantly equatorward in this region [*Nelson*, 1977]. On average, the slip is less than the maximum, so we expect that the mean meridional southward current is overestimated by ~1 cm s^{-1} and the mean zonal currents are not affected significantly. The spatial scales of the wind stress patterns are very broad south of ~40°N (except near the coast), so the statistics offshore, south of 40°N, are unlikely to be affected by the slip.

Following *Davis* [1991a], we compute the diffusivity via

$$\kappa_{jk}(\mathbf{x}, t) = -\langle v'_j(t_0|\mathbf{x}, t_0) d'_k(-t|\mathbf{x}, t_0) \rangle, \qquad (2)$$

where $\mathbf{v}'$ and $\mathbf{d}'$ are the departures from the Lagrangian mean velocity and displacement, respectively, and t_0 is the label for the time origin. The notation $v(t|\mathbf{x}_0, t_0)$ represents the value of v at time t of the particle passing through $\mathbf{x}_0$ at time t_0. We calculate this quantity as follows. Every data point in the area of interest (here the entire domain) is considered to label the origin of a pseudotrack with both negative and positive values for time. These are averaged as a function of time to yield the Lagrangian mean displacement $\mathbf{D}(t)$, from which we calculate $\mathbf{d}'(t) = \mathbf{d}(t) - \mathbf{D}(t)$ for each pseudotrack. We also require an

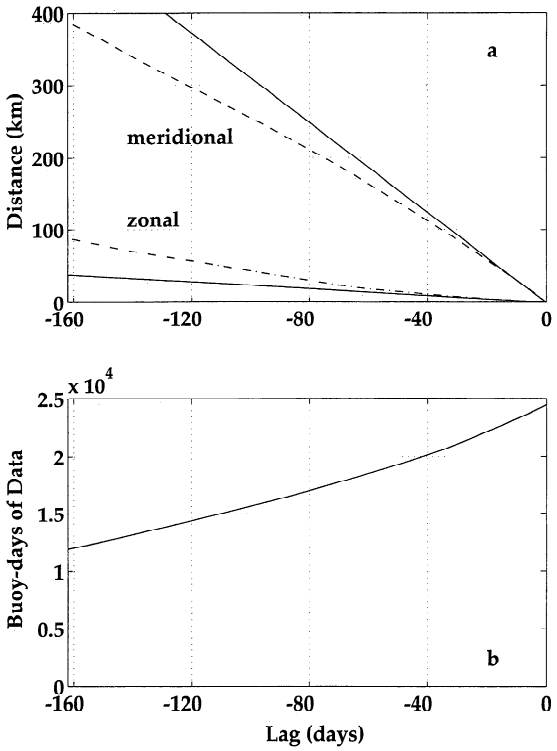

Figure 4. Estimates, based on the full data set, of (a) the Lagrangian mean displacement (dashed curve) and the displacements that would be obtained if the mean velocity were uniform (solid curve) and (b) the number of daily observations that are used for the estimates at each lag.

estimate of $\mathbf{v}'(t_0) = \mathbf{v}(t_0) - \mathbf{U}$ for each point in the area. The diffusivity $\kappa_{jk}(t)$ is estimated as the mean of the products $v'_j(t_0)d'_k(-t)$. The standard deviation of the sampling error for κ is approximately $\delta\kappa = 2(Kt/\mathrm{CAL})^{1/2}\kappa^{\infty}$, where CAL is the total extent of data (in buoy days, for example) upon which the estimate is based and K is a constant of ~4 [*Davis*, 1991a].

Figures 4 and 5 show the results of this calculation, where we limit attention to lags shorter than one quarter of the maximum lag [*Chatfield*, 1975]. This extends well beyond the range over which κ is expected to asymptote and is intended to demonstrate some of the difficulties that arise in estimating diffusivity as well as to provide some baseline estimates for the region. As expected, the mean displacement moves smoothly to the south and west (comes from the north and east). For small lags ($t <\approx 40$ days) the mean displacement is approximately linear. The curvature manifest at larger lags is a reflection of the underlying spatial variability of the mean velocity. This suggests that we need to interpret the behavior of the diffusivity for lags $>\sim$40 days with caution.

We discuss the diffusivity in terms of the diagonal components of the symmetric part of the diffusivity tensor, which are related to the dispersive effects of the unresolved flow, and the antisymmetric part of the diffusivity tensor, which describes the tendency of particles to veer [*Davis*, 1991a]. We begin with the symmetric part of the diffusivity tensor. Figure 5a shows the diagonal components of the symmetric part of the diffusivity tensor as a function of lag along with the sampling error of 2 standard deviations that roughly corresponds to a 95% confidence level. Notice that the estimates of the sampling error, which are given by $\delta\kappa = 2(Kt/\mathrm{CAL})^{1/2}\kappa^{\infty}$, grow with time like $t^{1/2}$. Other errors are introduced at long lags. The number of observations of $\kappa(t)$ decreases as t increases, which exacerbates the sampling error. Also, longer trajectories are more likely to sample regions that have different flow statistics. It is possible that the velocity fields in the California Current contain some very weak, long timescale variability that causes $\kappa(t)$ to vary slowly at large t, but it seems more likely that the large t behavior is a result of sampling errors and large-scale spatial inhomogeneity. For these reasons the expediency of truncating the covariance at a finite time where these errors are still small is quite reasonable.

Previous studies suggest that the Lagrangian integral timescale in this region is <10 days [*Poulain and Niiler*, 1989; *Brink et al.*, 1991]. Accordingly, we expect the diffusivity to asymptote to a constant value $\kappa^{\infty} = \lim_{t\to\infty} \kappa(t)$ by $t \approx 20$ days if the variability in the region is approximated by stationary and homogeneous turbulence. We may try to estimate (by eye) the asymptotic diffusivity based on $\kappa_{ii}(t)$ for lags <40 days (Figure 5b) where the zonal component asymptotes (within sampling error) to 4.2×10^7 cm^2 s^{-1} after $t \approx 5$ days and the meridional

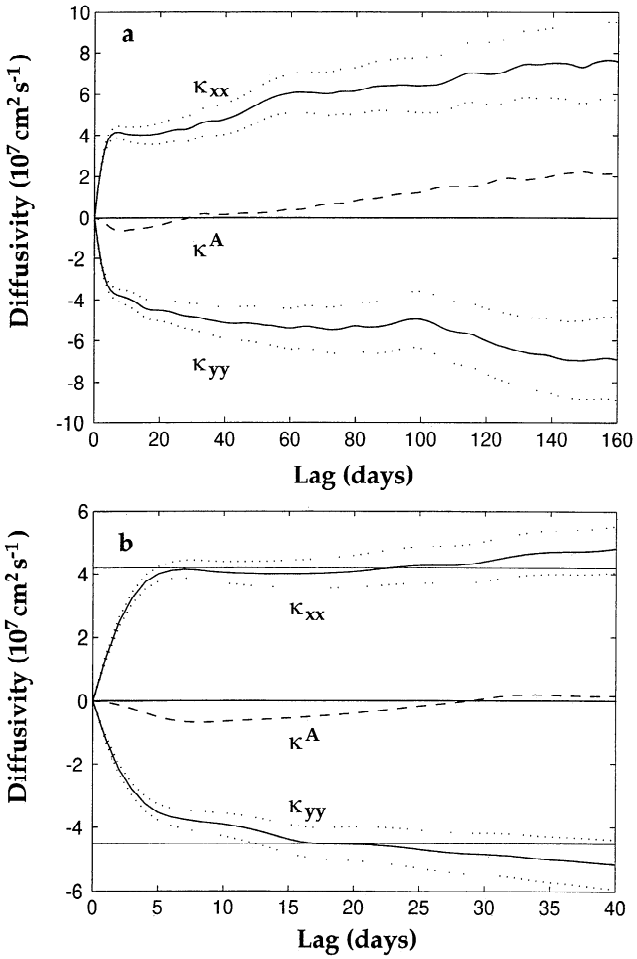

Figure 5. (a) Estimates, based on the full data set, of the zonal and meridional components of diffusivity and the antisymmetric component of the diffusivity tensor, $\boldsymbol{\kappa}^A$, and (b) a close-up of Figure 5a. The dotted curves indicate the sampling error estimate of 2 standard deviations, and the negative of κ_{yy} has been plotted for clarity. The thin horizontal lines, chosen by eye to estimate the asymptotic diffusivities, are at 4.2×10^7 and -4.5×10^7.

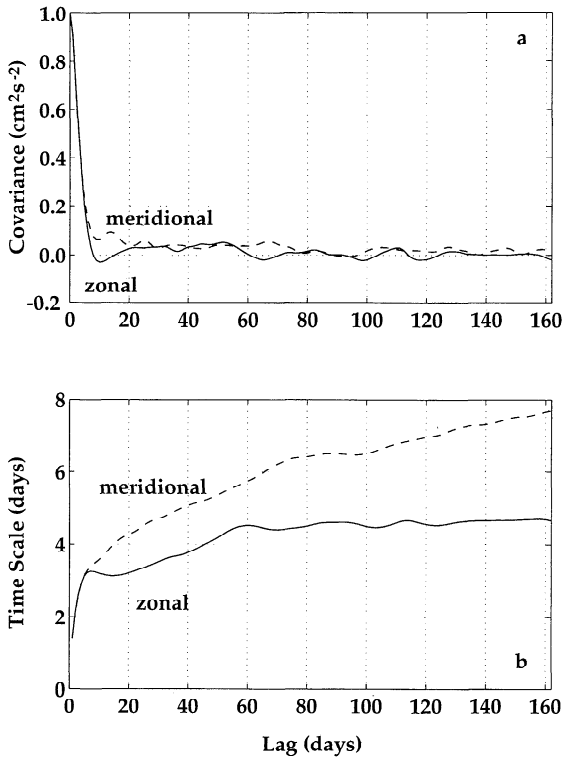

Figure 6. (a) Normalized mean time-lagged departure velocity products based on the full data set and (b) estimates of integral timescales as a function of integration range.

component, though growing slowly, asymptotes (within sampling error) to ~4.5 × 10^7 cm^2 s^{-1} after $t \approx 15$ days. The estimate of the Lagrangian timescale based upon the relationship $T = \kappa^\infty/\langle \nu'^2 \rangle$ leads to $(T_x, T_y) = (2.9, 3.5)$ days. The Lagrangian length scales, based on $L = \kappa^\infty \langle \nu'^2 \rangle^{-1/2}$, lead to $(L_x, L_y) = (32, 38)$ km. The square root of the sampling error variance of **U** is (0.19, 0.19) cm s^{-1}. The growth of the diffusivity curves for large lags is probably due to large-scale spatial variations in the mean that this calculation does not account for, so (4.2, 4.5) × 10^7 cm^2 s^{-1} probably represents a good estimate of the typical diffusivity for the region. This result is somewhat surprising because it suggests that the overall diffusivity is fairly well determined and nearly isotropic for the region despite clear evidence that the flow in the region displays significant nonstationarity and inhomogeneity.

Another view is presented by the mean time-lagged departure velocity products (autocovariance) $\langle u_i'(0) u_j'(\tau) \rangle$ (Figure 6). The e-folding scale of this statistic is between 3 and 4 days for both components, which is similar to previous estimates of decorrelation timescale in this region [*Poulain and Niiler*, 1989; *Brink et al.*, 1991]. The zonal component nearly asymptotes to zero after crossing zero at a lag of 8 days. The meridional component initially approaches zero very quickly but then begins to oscillate as it flattens out and does not cross zero until a lag of 90 days. The integral scale, if it exists, is the integral of the normalized covariance. We consider the sequence of estimates where the upper bound of the integration increases by 1 day for each member of the sequence. Figure 6b summarizes such a sequence and shows that while the timescale for the zonal component is fairly well determined with a value of ~4.5 days, the meridional component does not converge. Both the long lag until a zero crossing and the diverging integral timescale may arise from using a fixed mean velocity when the true mean velocity has spatial structure, which here is primarily manifest in the meridional component. This is related to the shape of the meridional diffusivity curve, which does not sharply plateau near 15 days the way the zonal component does near 5 days, and points to the conclusion that significant geographical variations of the flow properties exist.

The antisymmetric part of the diffusivity tensor, $\boldsymbol{\kappa}^A$, is associated with the tendency of particles to veer systematically during their history [*Davis*, 1991a, b; *Moffatt*, 1983]. We are unaware of any formal way to assess the sampling error for $\boldsymbol{\kappa}^A$, but the calculations (Figure 5) are suggestive. Here $\boldsymbol{\kappa}^A$ is negative out to ~30 days, which indicates a preference for positive mean angular momentum (cyclonic eddies) for time lags <~30 days. This is consistent with the results of *Poulain and Niiler* [1989]. The "terminal eddy" at 127°W, 37°N (Figure 1) is cyclonic and has a dominant effect on this calculation. Negative mean angular momentum begins to dominate for larger lags and may be the signature of the large-scale velocity field, which tends to turn westward after a time of southward drift (Figures 1, 7, and 11).

3.1.2. Eulerian maps: 5° × 5° resolution. It is more difficult to make Eulerian maps of diffusivity than of mean velocity. For velocity one simply sums up all of the velocity estimates for fixes that occurred within a specified area A. Diffusivity, on the other hand, is inherently nonlocal because it is defined as a correlation between the velocity departure at a point in A and the displacement-history departure during the time leading up to its arrival at the point in A. What portions of the track should be used in computing the correlation that is intended to describe the conditions in A? We determine the time window for which the mean displacement $\mathbf{D}(-t)$ remains in A and use that window on each pseudotrack to limit the lags used to characterize the conditions in A. We present the Lagrangian velocity statistics with a 5° × 5° resolution that, based on the size of the loops of the trajectories in Figure 1, we expect to be larger than the typical scale of the most energetic eddies but small enough to resolve significant large-scale variability. This is supported by *Poulain and Niiler* [1989], who estimated the dominant length scale of the eddy field to be 40–50 km. The calculations are the same as in the previous section, except we limit the extent of the tracks to be near the area of interest.

There are several caveats that apply to the interpretation of this mean velocity field. The mean velocity (Figure 7) must be interpreted with caution because the sampling density and time interval represented vary from one bin to the next. Also, because the velocity field influences the sampling array, there are three basic ways that Eulerian velocity statistics based on drifter observations can be biased [*Davis*, 1985]. There is an intrinsic correlation between particle position and velocity which can produce drift of constant level drogues in flows that are not horizontally nondivergent. The effect of convergences cannot be estimated [*Davis*, 1985]. Large-scale variation of drifter density, temporally and spatially, also introduces a bias of Eulerian averages. For example, a large number of drifters were intentionally deployed near the coast in a strong offshore flow near 39°N (Figure 1). They quickly exited the region and never returned. To the extent that the offshore flow they sampled is temporally variable, the result is biased because we have no drifter information about other times. On the edges of the drifter array a similar caveat applies because all samples are from buoys that arrived from the denser part of the array; none were available to come from the other direction. It is fortunate

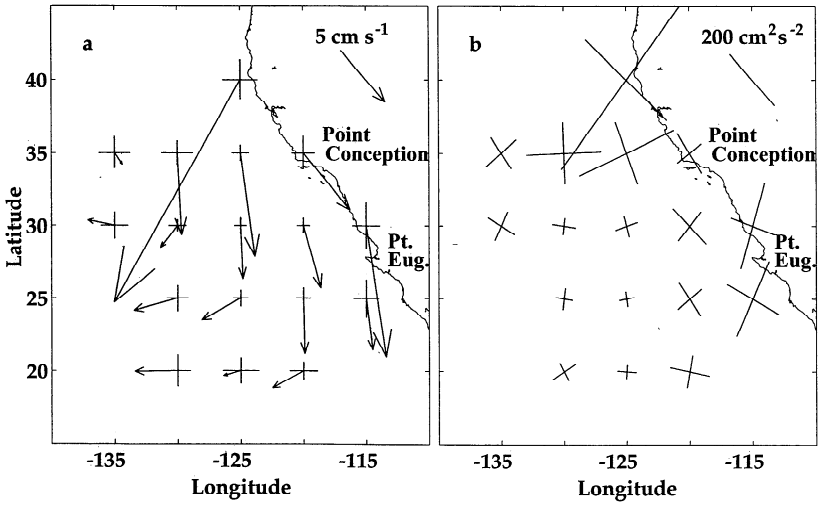

Figure 7. (a) Mean velocity and standard deviation and (b) principal axes of variance on a 5° × 5° resolution for bins with at least 360 buoy days of data.

that the correlation time of drifter velocity is short. This implies that a drifter's history, which determines its location, is poorly correlated with its present velocity so that, in general, this bias is not significant away from the edges of the domain defined by the drifter tracks. The third cause of bias in Eulerian averages derived from drifter data is inhomogeneity of the small-scale, eddy-dispersive velocity field, which causes a diffusive drift in Lagrangian trajectories even when the Eulerian mean of the velocity field is zero [*Freeland et al.*, 1975]. This is small, as it was in the Coastal Ocean Dynamics Experiment [*Davis*, 1985].

Finally, for regions where the flow is strong and/or there is high eddy variability, we have limited statistical reliability (sampling error). We estimate the standard error arising from this error source [*Davis*, 1991a] and plot it along with the mean velocity estimates in Figure 7. The velocity estimates in Figure 7 have also been corrected for array bias (Figure 8) based on the diffusivity estimates found later in this section, again following *Davis* [1991a]. This correction is proportional to $\nabla(\ln C)$, so it tends to be large only near the edges of the array where C is small. We depict only areas that have at least 360 buoy days of data, none of which are near the edges of the array, so the array bias corrections are all <3 cm s^{-1}. We see immediately that the mean velocity displays considerable structure (Figure 7). The northernmost bin shows a strong offshore flow that is a result of the deployment strategy used for CTZ87 and CTZ88. These experiments were designed to study strong offshore jets that form in the coastal transition zone each summer. Accordingly, the deployments were targeted for narrow, intense offshore jets. Most of the drifters deployed during these experiments were part of tight groups of buoys where about 10 buoys were deployed nearly simultaneously, separated by only a few kilometers [*Swenson et al.*, 1992]. This lowers the effective number of degrees of freedom for this bin, so the sampling errors associated with this bin are somewhat greater than those depicted in Figure 7. In any case it is unlikely that this is representative of the long-term mean, but taken at face value it represents a strong inhomogeneity in the mean and variance fields. Even if we disregard this effect, however, large-scale inhomogeneities are evident. The mean velocity is primarily equatorward near the shore and north of 22.5°N, while the flow turns westward in the offshore regions and south of 22.5°N. Longer lags in (2) preferentially sample the beginning and end of the buoy records. Since most of the offshore flow occurs near the end of the lives of the buoys, it is not surprising that we found the variability of κ for large lags that we noted in the last section. The variance also displays inhomogeneity with high values in the north and near Punta Eugenia (Figure 7b).

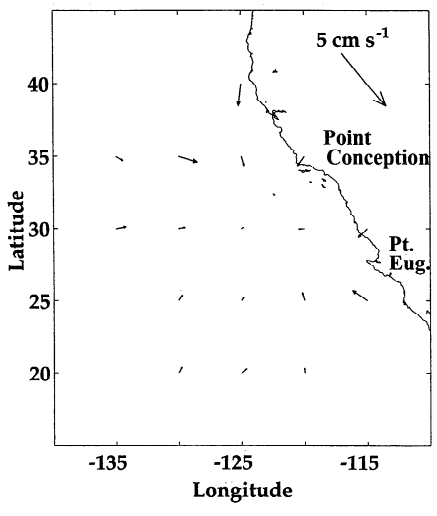

Figure 8. Estimates of array bias used to produce Figure 7.

We employ the F test [*Press et al.*, 1992] to determine whether there is significant anisotropy in the variance field. First, we decompose the velocity into components along and normal to the principal variance axes. After removing the sample mean we estimate for each bin the number of degrees of freedom by $N\Delta t/(2T_{\max})$, where $T_{\max}$ is the maximum of the zonal and meridional Lagrangian timescale estimates for the bin, N is the number of samples in the bin, and Δt is the sampling interval. For the three bins with peaked diffusivity curves (Figure 10) we use the maximum value of $\kappa(t)$ to compute the timescale, which effectively produces an upper bound for the timescale. The null hypothesis that the time series of the two velocity components were drawn from normal

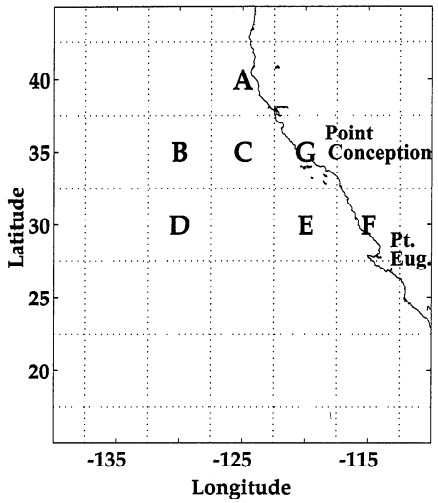

Figure 9. Geographical location of the bins with statistically significant anisotropy.

distributions with the same variance is rejected with 95% confidence for six of the bins (Figure 9): bin A, 40°N, 125°W; bin B, 35°N, 130°W; bin C, 35°N, 125°W; bin D, 30°N, 130°W; bin E, 30°N, 120°W; and bin F, 30°N, 115°W. In addition, the null hypothesis is rejected at the 90% confidence level for the coastal bin G, 35°N, 120°W. The northwestern three bins (A, B, and C) are strongly influenced by the experiment design which required that the buoys be deployed in a strong offshore jet in this region. Although this may be a recurrent feature, the data here are dominated by one intense realization, and this cannot be considered typical. Two of the bins (F and G) are coastal bins where the ocean occupies less than half of their area, which indicates that the coastal boundary produces the anisotropy. The remaining two bins are the most interesting. Bin D encompasses the region where the subarctic and northern subtropical fronts approach the California Current [*Lynn*, 1986]. Six buoys turned westward into the frontal region and continued out to 140°W. The frontal region is oriented east-west, so zonal excursions are more energetic than meridional ones. The final bin (bin E) appears to be influenced by the coast as most of the data in bin E are <250 km from the shore, and the axis of strongest variability is aligned with the coastline.

The plot of $\kappa(t)$ as a function of longitude and latitude (Figure 10) yields some powerful insights. In regions where $\kappa(t)$ reaches a stable value quickly, we can be confident that a traditional advection-diffusion model with eddy diffusivity κ^{∞} will adequately describe the evolution of large-scale passive tracer fields such as sea surface temperature. This behavior is found in all bins to the west and south of 30°N, 120W. Regions where $\kappa(t)$ levels out for short lags and then meanders for larger lags indicate that significant inhomogeneities exist within the 5° × 5° bin. We see this behavior in the two coastal bins along 115°W, where the presence of the coast introduces spatial inhomogeneity. Longer lag meandering of $\kappa(t)$ also occurs in the bin at 35°N, 135°W. Regions where $\kappa(t)$ is sharply peaked require closer analysis. Sharply peaked $\kappa(t)$ is found only for bins in the range (132.5°W–122.5°W and 32.5°N–42.5°N) for which we have three separate curves. This is a region that includes the jet and the long-lived "terminal" eddy (Figure 1) [*Strub et al.*, 1991; *Swenson et al.*, 1992]. As we discussed before, the deployment strategy used for these experiments indicates that the results from this region cannot be considered typical. This peaked behavior in the diffusivity curve is apparently due to the domination of eddy or looping structures in the data sample. This raises serious questions about how to interpret the results. If we could observe $\kappa(t)$ out to a lag where it finally does asymptote, we could use the generalized advection-diffusion model [*Davis*, 1987] and the variable $\kappa(t)$ to assess the effect it has on the evolution of the mean field. Errors in the estimate grow with time, however, and we are not able to observe the (hoped for) flattening out

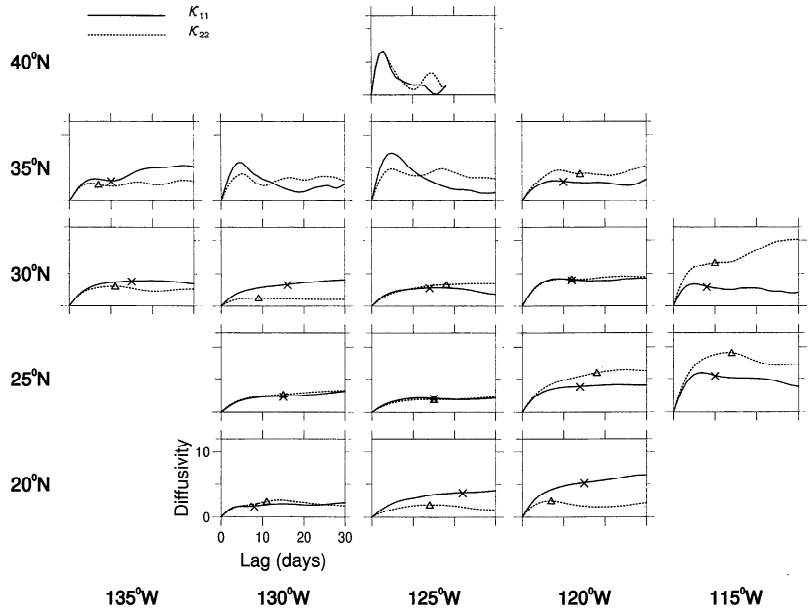

Figure 10. Estimates of the zonal (solid curves) and meridional (dashed curves) diffusivity in units of 10^7 $cm^2\ s^{-1}$, as a function of lag for 5° × 5° bins. Symbols indicate the value which is taken to be κ^{∞}. Panels without symbols indicate regions where a simple "flux versus gradient" relation is unlikely to be useful. The lower left-hand panel exhibits the axes labels that are shared by all of the panels.

Table 2. Estimates of Zonal Variance With Estimates of the 95% Confidence Interval for Each 5° × 5° Bin With at Least 360 Buoy Days of Data

	Longitude				
Latitude	135	130	125	120	115
40	x	x	X	x	x
35	117 ± 19	X	X	106 ± 13	x
30	95 ± 15	75 ± 9	73 ± 6	126 ± 8	155 ± 19
25	x	54 ± 9	49 ± 6	100 ± 9	192 ± 20
20	x	77 ± 13	61 ± 16	124 ± 18	x

Estimates are in $cm^2\ s^{-2}$. Capital Xs denote bins that have at least 360 buoy days of data but which are not likely to obey a "flux versus gradient" relation.

Table 3. Estimates of Meridional Variance With Estimates of the 95% Confidence Interval for Each 5° × 5° Bin With at Least 360 Buoy Days of Data

	Longitude				
Latitude	135	130	125	120	115
40	x	x	X	x	x
35	113 ± 16	X	X	120 ± 18	x
30	90 ± 12	46 ± 4	62 ± 6	123 ± 8	237 ± 35
25	x	60 ± 10	43 ± 5	106 ± 11	221 ± 27
20	x	65 ± 13	40 ± 8	94 ± 9	x

Estimates are in $cm^2\ s^{-2}$. Capital Xs denote bins that have at least 360 buoy days of data but which are not likely to obey a "flux versus gradient" relation.

to within sampling error. Also, if buoys leave the area far behind, they no longer characterize that area. Basically, we only know the short-time, variable $\kappa(t)$ from observations. The parameter $Hi = T/T_c$, where T_c is the timescale on which Θ varies and T is the Lagrangian timescale, measures the relative importance of the history correction to the total eddy flux. For those cases where $\kappa(t)$ does not equilibrate quickly, T may be large, and the history corrections to a "flux versus gradient law" will be relatively important in the transport of passive tracers.

As we discussed, the most accurate determinations of the asymptotic diffusivity $\kappa^\infty = \lim_{t\to\infty} \kappa(t)$ are made by estimating $\kappa(t)$ at the smallest lag for which $\kappa(t) \approx \kappa^\infty$ [*Davis*, 1991a]. We make these determinations objectively via the following procedure. We estimate $\kappa(t)$ for each 5° × 5° bin based on only those parts of the pseudotracks that stay within 2.5° of each pseudoorigin. An initial estimate for κ^∞ is determined as the value of $\kappa(t)$ at the lag that is one quarter of the maximum lag calculated for the box [*Chatfield*, 1975]. We use these values along with variance estimates to estimate the integral timescales and length scales. An improved estimate for κ^∞ is evaluated at $3T$ rounded up to the next integer, where T is the integral timescale. This corresponds to the lag at which κ would reach 95% of κ^∞ if the velocities were governed by a Markovian process. Estimates for the timescales are adjusted to reflect the new estimates of κ^∞, and the process is repeated until the values for κ^∞ and T are consistent. The results are checked a posteriori against the assumption that $T <\approx 20$ days. We also inspect each history $\kappa(t)$ to determine the extent to which it behaves according to our expectations. Following *Davis* [1991a], we determine the standard error for the mean velocity estimate as a function of the number of observations, estimated diffusivity, and estimated integral length scale. In regions where $\kappa(t)$ is peaked, this provides an upper bound on the sampling error.

Tables 2–9 display the variances, diffusivities, and integral scales for each bin. The outstanding feature in the variance is the strong westward gradient in both zonal and meridional variances out to 125°W (Tables 2 and 3). Each component has a band of small values that runs diagonally from 30°N, 130°W southeastward to 20°N, 125°W, although the distinct anisotropy at 30°N, 130°W causes the zonal and meridional components to have slightly different spatial structure. The estimates of diffusivity are accompanied by error estimates that make geographical variations difficult to identify with confidence at the 95% level (Tables 4 and 5). Nonetheless, there are notable exceptions. First, there is a significant drop-off of meridional diffusivity westward of 30°N, 125°W and both westward and southward of 25°N, 120°W. Second, the zonal diffusivity at 30°N, 120°W and 25°N, 115°W is significantly higher than that farther offshore at 25°N, 125°W and 20°N, 130°W. Notice that 30°N, 130°W, where the flow is anisotropic, is a minimum for meridional diffusivity.

The zonal timescale and length scale, T_x and L_x, respectively, do not demonstrate significant spatial variability (Tables 6 and 8). The meridional scales display a more complicated structure. The meridional timescale and length scale, T_y and L_y (Tables 7 and 9), indicate that those in the area to the north and east of 30°N, 125°W and 25°N, 120°W are greater than those in the south and west of that region. In particular, significant gradients exist along 30°N between 125°W and 130°W and along 120°W between 25°N and 20°N for both the timescale and length scale. These measurements indicate that for the meridional component, there is a band roughly 1000 km offshore where the variance level (relative to the diffusivity) increases and suggests that the variability is dominated by processes with a shorter timescale or space scale or both.

A persistent question in the literature is the following: Can the diffusivity be related to the scales of motion of the random velocity field? *Rossby et al.* [1983] suggest $\kappa^\infty \propto u_0^2 T$, where u_0^2 is the velocity variance and T, the integral timescale, was approximately constant over the range of ocean conditions examined. Different observations led *Krauss and Boning* [1987] to suggest $\kappa^\infty \propto u_0 L$, where the characteristic length L was nearly constant. Finally, *Keffer and Holloway* [1988] suggest $\kappa^\infty \propto \psi_0$, where ψ_0 is the standard deviation of the stream function perturbation associated with quasi-geostrophic eddies. As pointed out by *Davis* [1991a], these must be regarded

Table 4. Estimates of Zonal Diffusivity With Estimates of the 95% Confidence Interval for Each 5° × 5° Bin With at Least 360 Buoy Days of Data

	Longitude				
Latitude	135	130	125	120	115
40	x	x	X	x	x
35	3.1 ± 1.8	X	X	3.0 ± 1.3	x
30	3.8 ± 2.2	3.3 ± 1.4	2.8 ± 0.8	4.1 ± 1.0	3.0 ± 1.4
25	x	2.3 ± 1.3	2.0 ± 0.9	3.8 ± 1.2	5.5 ± 2.0
20	x	1.7 ± 1.0	3.8 ± 3.4	5.2 ± 2.6	x

Estimates are in units of $10^7\ cm^2\ s^{-1}$. Capital Xs denote bins that have at least 360 buoy days of data but which are not likely to obey a "flux versus gradient" relation.

Table 5. Estimates of Meridional Diffusivity With Estimates of the 95% Confidence Interval for Each 5° × 5° Bin With at Least 360 Buoy Days of Data

	Longitude				
Latitude	135	130	125	120	115
40	x	x	X	x	x
35	2.3 ± 1.1	X	X	4.6 ± 2.4	x
30	2.7 ± 1.3	1.1 ± 0.3	3.2 ± 1.0	4.2 ± 1.0	6.5 ± 3.4
25	x	2.5 ± 1.5	1.8 ± 0.8	5.4 ± 1.9	8.7 ± 3.7
20	x	2.0 ± 1.4	1.5 ± 1.1	1.7 ± 0.6	x

Estimates are in units of 10^7 cm^2 s^{-1}. Capital Xs denote bins that have at least 360 buoy days of data but which are not likely to obey a "flux versus gradient" relation.

Table 7. Estimates of Single-Sided Meridional Timescale With Estimates of the 95% Confidence Interval for Each 5° × 5° Bin With at Least 360 Buoy Days of Data

	Longitude				
Latitude	135	130	125	120	115
40	x	x	X	x	x
35	2.3 ± 1.2	X	X	4.4 ± 2.4	x
30	3.5 ± 1.8	2.7 ± 0.9	5.9 ± 2.0	3.9 ± 1.0	3.2 ± 1.7
25	x	4.9 ± 3.0	4.9 ± 2.2	5.9 ± 2.2	4.6 ± 2.0
20	x	3.5 ± 2.5	4.4 ± 3.3	2.1 ± 0.7	x

Estimates are in days. Capital Xs denote bins that have at least 360 buoy days of data but which are not likely to obey a "flux versus gradient" relation.

as proposals only for fully nonlinear turbulence and may be made equivalent by taking $L = \psi_0/u_0$ and $T = \psi_0/u_0^2$, which is the eddy turnaround time (i.e., the time it takes a typical particle to go around a typical eddy once). For the latter scaling the distinction between the proposals amounts to the degree to which L and T vary over the conditions encountered. Because there are no significant gradients in the zonal component of either T or L, the zonal residual velocities are consistent with both of the scalings $\kappa^\infty \propto u_0^2 T$ and $\kappa^\infty \propto u_0 L$. Consequently, it may be useful to think of these residual velocities as fully nonlinear turbulence.

To explore this issue more fully, we fit regression curves to the relationship between the components of diffusivity and variance as (1) a straight line and (2) as a quadratic using the error estimates for both components [*Press et al.*, 1992]. The results of this regression can be interpreted as support (or not) for an implied model that (1) the integral timescale or (2) the integral length scale is constant over the range of conditions encountered [*Poulain and Niiler*, 1989; *Figueroa and Olson*, 1989]. First, we consider the zonal component. The results vary depending on whether the two boundary bins, (120°W, 35°N) and (115°W, 30°N), are included in the analysis. When the boundary bins are included, the goodness-of-fit estimates [*Press et al.*, 1992] are 0.32 and 0.33 for models 1 and 2, respectively. On the other hand, when the boundary bins are excluded from the analysis, we obtain goodness-of-fit estimates of 0.55 and 0.55, respectively (Figure 11). For the latter case the regression constants indicate that the single-sided integral timescale and length scale are $T = 3.1 \pm 0.7$ days and $L = 52 \pm 11$ km, respectively. Figure 11 also depicts the boundary bin values and the regression curves obtained by including them in the analysis. It appears that the bin at 25°N, 115°W is not compatible with either of models 1 or 2. This indicates that the dynamics that produce the variability in this bin are different from those that govern the rest of the domain. This is clear in Figure 1, where we see that Baja California occupies more than half of the bin and is a barrier to zonal excursions. The other boundary bin is compatible with the rest of the domain, primarily because most of the data for this bin are in the Southern California Bight, which extends to the easternmost limit of this bin. The comparable timescale and length scales given by *Poulain and Niiler* [1989] were 4.6 ± 1.3 days and 39 ± 13 km, which is not inconsistent with the new estimates. As may be expected from the gradients discerned in the timescale and length scale for the meridional component in Tables 7 and 9, the regression is not successful for the meridional component. The goodness-of-fit estimates for models 1 and 2 are 3.7×10^{-4} and 1.0×10^{-4}, respectively. One possible interpretation is that the error estimates are too small, but the error estimates would need to be increased by a factor of 1.8 to produce goodness-of-fit values as high as 0.5. If, as *Davis* [1991a] has suggested, hypotheses 1 and 2 are based on fully developed turbulence, locations where hypotheses 1 and 2 fail may indicate places where the ocean is not characterized by fully developed turbulence. This suggests that the meridional velocity departures result from a flow regime that is organized by, for example, wave-like motion or coherent structures.

There are no cases where the hypotheses underlying models 1 or 2 can be distinguished. This was found in other studies as well [*Figueroa and Olson*, 1989; *Poulain and Niiler*, 1989], which suggests that the timescale and space scales vary in a complimentary way and provides support for *Davis*'s [1991a] hypoth-

Table 6. Estimates of Single-Sided Zonal Timescale With Estimates of the 95% Confidence Interval for Each 5° × 5° Bin With at Least 360 Buoy Days of Data

	Longitude				
Latitude	135	130	125	120	115
40	x	x	X	x	x
35	3.0 ± 1.9	X	X	3.3 ± 1.5	x
30	4.7 ± 2.8	5.2 ± 2.2	4.5 ± 1.4	3.7 ± 0.9	2.2 ± 1.1
25	x	4.9 ± 3.0	4.7 ± 2.1	4.4 ± 1.5	3.3 ± 1.3
20	x	2.5 ± 1.5	7.1 ± 6.9	4.9 ± 2.5	x

Estimates are in days. Capital Xs denote bins that have at least 360 buoy days of data but which are not likely to obey a "flux versus gradient" relation.

Table 8. Estimates of Single-Sided Zonal Length Scale With Estimates of the 95% Confidence Interval for Each 5° × 5° Bin With at Least 360 Buoy Days of Data

	Longitude				
Latitude	135	130	125	120	115
40	x	x	X	x	x
35	28 ± 17	X	X	29 ± 13	x
30	40 ± 23	39 ± 16	33 ± 10	36 ± 9	24 ± 11
25	x	31 ± 18	28 ± 12	38 ± 12	40 ± 15
20	x	19 ± 11	48 ± 45	47 ± 24	x

Estimates are in kilometers. Capital Xs denote bins that have at least 360 buoy days of data but which are not likely to obey a "flux versus gradient" relation.

Table 9. Estimates of Single-Sided Meridional Length Scale With Estimates of the 95% Confidence Interval for Each 5° × 5° Bin With at Least 360 Buoy Days of Data

	Longitude				
Latitude	135	130	125	120	115
40	x	x	X	x	x
35	21 ± 11	X	X	42 ± 22	x
30	29 ± 14	16 ± 5	40 ± 13	37 ± 9	42 ± 22
25	x	33 ± 19	28 ± 12	52 ± 19	59 ± 25
20	x	25 ± 17	24 ± 18	17 ± 6	x

Estimates are in kilometers. Capital Xs denote bins that have at least 360 buoy days of data but which are not likely to obey a "flux versus gradient" relation.

esis that the distinction between the proposals amounts to the different degree to which L and T vary over the conditions encountered.

For lags of $<\sim$20 days the pattern of $\boldsymbol{\kappa}^A$ (Figure 12) depicts the influence of cyclonic eddies on the paths of the drifters. Only near the coast or in the bins at 25°N, 130°W and 20°N, 125°W do the drifters reflect the influence of anticyclonic eddies. The overall pattern indicates that cyclonic eddies dominate the mesoscale signature of the drifters as noted by *Poulain and Niiler* [1989]. Here we show that this tendency is ubiquitous over the well-sampled area. This may arise either because (1) cyclonic eddies outnumber anticyclonic eddies or (2) cyclonic (anticyclonic) eddies are convergent (divergent) and therefore cyclonic eddies are preferentially sampled by drifters. Regions of previous net convergence are regions of cyclonic vorticity for quasi-geostrophic motions [*Middleton and Garrett*, 1986], which is consistent with the latter hypothesis. We cannot distinguish between these two possibilities with the drifter data alone.

3.2. Joint Velocity-Temperature Statistics

What effects do the eddy motions have on heat transport? As mentioned in section 2, we do not expect that absolute values of the temperatures can be meaningfully compared between the drifters considered in this study. This creates a difficulty because we would like to estimate the eddy heat flux divergence $\nabla \cdot \langle \mathbf{u}'\theta' \rangle$, which requires an estimate of the mean temperature Θ so that $\theta' = \theta - \Theta$ can be determined. Furthermore, both the temperature and velocity undergo sizable seasonal variations that we do not want to include in our estimate of eddy heat flux divergence. Accordingly, we develop a filter with sharp spectral characteristics designed to minimize leakage between the low- and high-frequency regimes that includes a spectral gap to ensure that the filtered time series are essentially independent (Figure 13). These filtered time series are used to compute estimates of the eddy statistics and to derive confidence levels. The basic velocity statistics from the filtered data compare favorably with those determined in the straightforward way.

First, we compare the velocity statistics of the subset with those of the full data set to determine the extent to which this subset may differ from the full data set. Only ~40% of the drifter data set provided temperature records that are useful for this study (Figure 2). These temperature records are confined to 1988–1989. They have a seasonal distribution similar to that of the full data set (Figure 2b) and provide more limited spatial coverage, particularly south of 30°N (Figure 1b). The overall mean velocity for the limited data set is $\mathbf{U} = (0.0, -4.7)$ cm s^{-1} based on 9900 daily samples. Compared with estimates based on the full data set, this is faster southward by 0.7 cm s^{-1} and does not show a weak offshore mean velocity. Variances about the mean are $\langle u'u' \rangle = 191$, $\langle v'v' \rangle = 151$, and $\langle u'v' \rangle = 23$ cm^2 s^{-2}, the first two of which correspond to root mean square speeds of 14 and 12 cm s^{-1}. A principal axes decomposition yields a major (minor) axis of 201 (141) cm^2 s^{-2} with the major

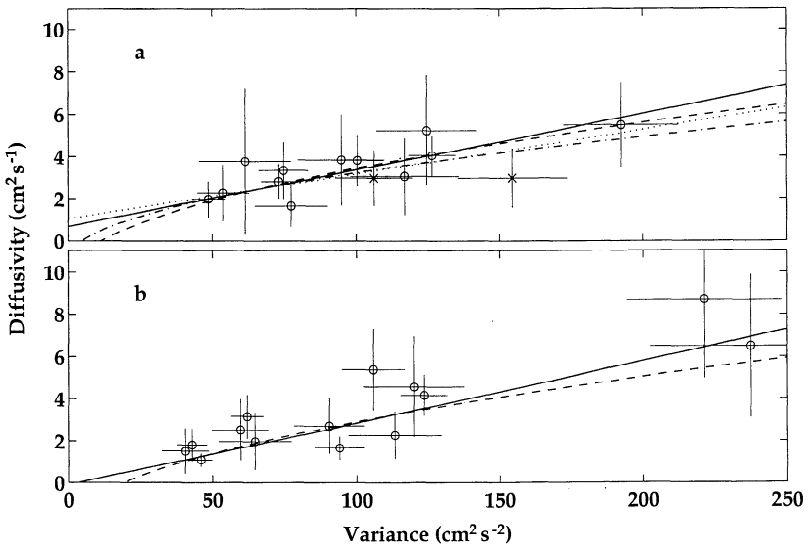

Figure 11. Plots of diffusivity versus variance for (a) the zonal component and (b) the meridional component. Regression results for a linear relationship (solid curves) and a quadratic relationship (dashed curves) are superimposed. For Figure 11a the regression curves are for the case where the boundary bins (denoted by a cross) are excluded. The regression curves where the boundary bins are included are shown for comparison (linear, dotted curve; quadratic, dash dotted curve). The lines centered on each point represent approximate 95% confidence limits.

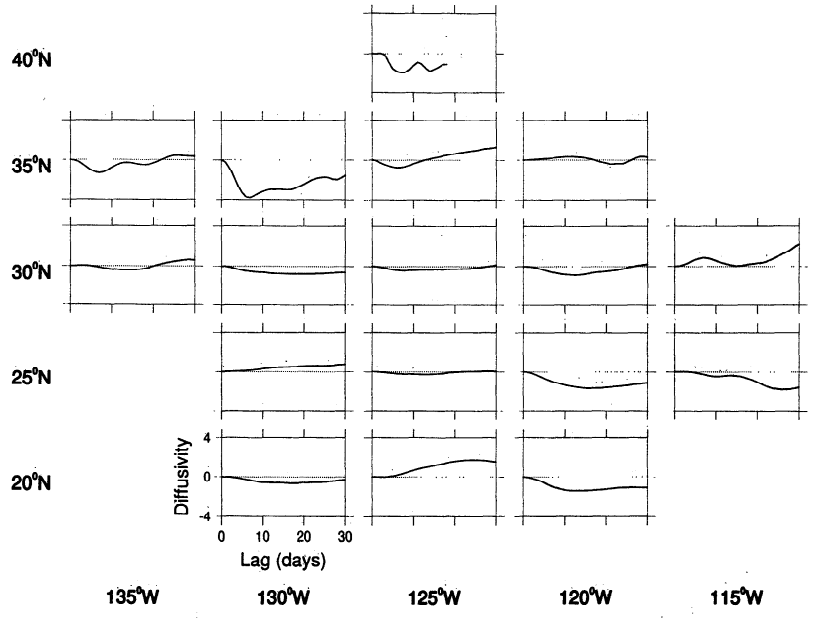

Figure 12. Estimates of the antisymmetric part of the diffusivity tensor in units of 10^7 cm^2 s^{-1}, as a function of lag for 5° × 5° bins. The lower left-hand panel exhibits the axes labels that are shared by all of the panels.

axis aligned along $\theta = 24°$, where $\theta = 0°$ is due east. These values are very close to those from the full data set, although the variances are somewhat higher. The diffusivity tensor has only minor differences from that determined from the full data set.

We calculate a separate mean $\mathbf{u}$ and θ for each drifter and subtract the value to obtain velocity and temperature departures for each buoy. The first and last 30 days of each of the departure time series are tapered with a Blackman window, and the residual mean values are subtracted to produce the final departure time series. These departure time series provide a basis for a conservative estimate of the heat flux owing to variations at all observed frequencies. Elliptic filters of order 6 are used to extract low-pass (60-day periods and greater) and high-pass (30-day periods and less) components (Figure 13). Eddy statistics are accumulated on a 2° × 2° grid in order to facilitate the calculation of derivatives needed to make estimates of the divergence; lower resolutions do not allow such estimates to be made. The significance of each correlation $\langle \mathbf{u}'\theta' \rangle$ is assessed by calculating the rank correlation and keeping only those values that are different from zero at a 95% confidence level. The number of degrees of freedom used to determine the 95% confidence level is $N\Delta t/(2T) - 2$ [*Riser and Rossby*, 1983; *Press et al.*, 1992], where N is the number of samples in the region, Δt is the sampling interval, and T is an estimate of the typical Lagrangian timescale, taken to be 5 days.

We consider three cases: (1) the full departure time series, which accounts for all of the observed velocity-temperature covariance, (2) the low-pass component, which roughly accounts for the seasonal covariance, and (3) the high-pass component, which roughly accounts for the covariance of the mesoscale. The results are marginally significant because the data density is also marginal. Significant estimates of $\langle \mathbf{u}'\theta' \rangle$ all lie within the region 25°N–37°N and 130°W–116°W, which comprises 56 2° × 2° bins. Case 1, for example, produces 28 different estimates (statistically different from zero) of the components of $\langle \mathbf{u}'\theta' \rangle$ (out of a possible 2 × 56 = 112), but only

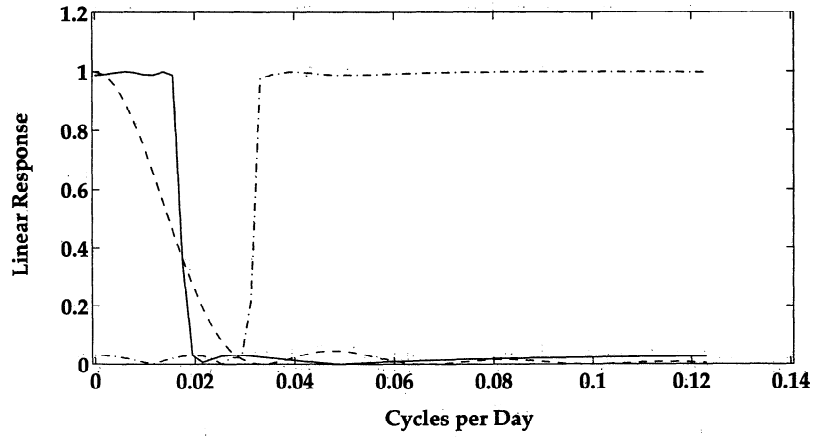

Figure 13. Linear response of the filter used to estimate the eddy variability of $\mathbf{u}$ and T from individual drifters. Solid curve denotes the low-pass filter, and dash-dotted curve denotes the high-pass filter. The linear response of a 31-day triangle filter (dashed curve) is presented for comparison.

Table 10. Direct Drifter-Based Estimates of the Eddy Heat Flux Divergence in the California Current

Case	$\partial_x\langle u'\theta'\rangle$, 10^{-8} °C s^{-1}	$\partial_y\langle v'\theta'\rangle$, 10^{-8} °C s^{-1}	$\nabla\cdot\langle\mathbf{u}'\theta'\rangle$, 10^{-8} °C s^{-1}	Region	Number of Estimates
Full filtered data	3.4	−0.1	3.3	(129°–119°W, 29°–37°N)	12
Low pass	2.8	−1.2	1.6	(129°–119°W, 29°–36°N)	14
High pass	1.4	−0.7	0.8	(126°–124°W, 30°–36°N)	7

Low pass (high pass) refers to periods > (<) 60 (30) days. For comparison the mean heat flux divergence, estimated from the currents in Figure 7 and the long-term SST climatology, is 12×10^{-8} °C s^{-1} (see text).

nine bins have estimates for both components, and these nine are scattered. Accordingly, our estimates of divergence rely on zonal first differences of adjacent significant estimates of $\langle u'\theta'\rangle$ and meridional first differences of adjacent significant estimates of $\langle v'\theta'\rangle$. The results (Table 10) imply that during 1988 and 1989 the eddy heat flux divergence in the upper ocean in the California Current during summer and fall is ~1–3 × 10^{-8} °C s^{-1}. The eddy heat flux divergence associated with the high-pass band is smaller than that associated with the full records by a factor of 4, but this result must be viewed with caution because it is based on very few reliable estimates of the differences between adjacent eddy heat flux estimates.

These values for the eddy heat flux divergence may be compared to the results obtained by particle statistics alone. The usual choice for the parameterization of the horizontal turbulent fluxes by eddy diffusivity is $\nabla\cdot\langle\mathbf{u}'\theta'\rangle = \nabla(\kappa\nabla\Theta)$. This may be regarded as arising from mesoscale variability. From our data, gradients of κ cannot be confidently estimated, but we can make an order of magnitude estimate of the term based on a typical value for κ (4×10^7 cm^2 s^{-1}; see Tables 4 and 5) and the value for $\nabla^2\Theta$ based on the sea surface temperature (SST) climatology in the area (2×10^{-12} °C m^{-2}) [*Reynolds and Smith*, 1995], yielding an order of magnitude estimate for $\kappa\nabla^2\Theta$ of 0.8×10^{-8} °C s^{-1}, which is, perhaps coincidentally, in excellent agreement with the direct estimate for the eddy heat flux divergence from the high-pass (mesoscale) band.

How do these values compare with estimates for the long-term mean of the other terms in the advection-diffusion equation for this region? The climatological net downward surface heat flux is nearly zero in this region, with positive values near the coast being offset by negative values offshore [*Oberhuber*, 1988]. The mean heat flux divergence, based on the currents in Figure 7 (not including the three bins with peaked diffusivities in Figure 10) and the long-term SST climatology in the area, is 12×10^{-8} °C s^{-1}. If we assume that the mean and eddy heat flux divergences act uniformly over a mixed layer of depth 50 m, we find that the mean heat flux divergence, which is dominated by $V\partial_y\Theta$, amounts to ~20 W m^{-2} and the eddy heat flux divergence amounts to a heating rate of 2–6 W m^{-2}. Therefore the mean heat flux divergence is quite significant for the long-term upper ocean heat balance, while the eddy heat flux divergence does not appear to be a significant factor.

4. Conclusions

We use *Davis*'s [1991a] approach to estimate the basic transport processes based on Lagrangian drifters in the California Current during 1985–1990. The theoretical foundation of the method is much stronger when the departure statistics of the velocities are approximately Gaussian, and we show that, except near the coast, the hypothesis that the velocity departures are Gaussian cannot be rejected at the 95% confidence level. We obtain estimates of the mean fields of velocity and variance as well as geographically varying estimates of diffusivity, integral timescales, and integral space scales, including estimates of sampling errors for each of these quantities. Some geographical variations of these fields emerged as significant: (1) There is a strong westward gradient in both zonal and meridional variance out to 135°W, (2) each variance component has a band of small values that runs diagonally southeastward from 30°N, 130°W to 20°N, 125°W, (3) there is a distinct anisotropy at 30°N, 130°W, which is the region where deep-ocean frontal systems approach the California Current, (4) meridional diffusivity experiences a significant drop-off to the west of 30°N, 125°W and to the south and west of 25°N, 120°W, (5) zonal diffusivity declines significantly from the northeast to the southwest, (6) zonal integral timescales and space scales show no significant geographical variation, which suggests that zonal departure velocities may be usefully thought of as fully nonlinear turbulence, and (7) meridional integral timescales and space scales show a distinct minimum ~1000 km offshore, which indicates that the variability is dominated by processes with shorter timescales or space scales or both.

We also determine regions where the "flux versus history-of-gradient relation" derived by *Davis* [1991a] may be important. This is manifest by short, sharply peaked diffusivity curves (Figure 10). Recall that *Brink et al.* [1991] found diffusivities with sharp peaks; such regions cannot be interpreted in terms of a simple "flux versus gradient" relation. The antisymmetric part of the diffusivity tensor relates to the preferred sense of rotation, and we find that the influence of cyclonic eddies on the paths of the drifters is dominant.

We seek simple parameterizations to relate the scales of motion of the random velocity field to the diffusivity by fitting regressions to $\kappa^\infty \propto u_0^2 T$ and $\kappa^\infty \propto u_0 L$, where u_0^2 is the velocity variance. In no case could these two hypotheses be distinguished. The goodness of fit for the zonal component depends strongly on whether the coastal bins are included in the analysis: The region 25°N, 115°W is not compatible with either of the hypotheses. Otherwise, both models obtain good fits. The regression is not successful for the meridional component. This suggests that the meridional departure velocities result from a flow regime that is significantly organized by, for example, waves or coherent structures.

Finally, we produce the first direct estimates of the horizontal eddy heat flux divergence based on Lagrangian estimates. The "eddy diffusivity" parameterization of the eddy heat flux divergence $\nabla\cdot\langle\mathbf{u}'\theta'\rangle = \nabla(\kappa\nabla\Theta)$ is computed separately based on the estimates of diffusivity contained herein and a sea sur-

face temperature climatology [*Reynolds and Smith*, 1995]. The independently calculated terms agree well, which provides a measure of reassurance about the diffusivity estimates. The magnitude of the eddy heat flux divergence in the California Current is very small (<5 W m^{-2}) and does not appear to be significant in the long-term heat budget of the upper ocean in this region.

Acknowledgments. M. S. S. thanks Jeff Paduan, Annalisa Griffa, and Don Hansen for many beneficial discussions. We are also indebted to anonymous reviewers who helped to improve the manuscript. This work was supported in part by ONR grant N00014-89-J-1241 and by NOAA/OGP grant EN180-94.

References

Allen, J. S., L. J. Walstad, and P. A. Newberger, Dynamics of the coastal transition zone jet, 2, Nonlinear finite amplitude behavior, *J. Geophys. Res.*, *96*, 14,995–15,016, 1991.

Brink, K. H., and T. J. Cowles, The Coastal Transition Zone Program, *J. Geophys. Res.*, *96*, 14,637–14,647, 1991.

Brink, K. H., R. C. Beardsley, P. P. Niiler, M. Abbott, A. Huyer, S. Ramp, T. Stanton, and D. Stuart, Statistical properties of near-surface flow in the California coastal transition zone, *J. Geophys. Res.*, *96*, 14,693–14,706, 1991.

Chatfield, C., *The Analysis of Time Series: Theory and Practice*, Chapman and Hall, New York, 1975.

Davis, R. E., Drifter observations of coastal surface currents during CODE: The statistical and dynamical views, *J. Geophys. Res.*, *90*, 4756–4772, 1985.

Davis, R. E., Modeling eddy transport of passive tracers, *J. Mar. Res.*, *45*, 635–666, 1987.

Davis, R. E., Observing the general circulation with floats, *Deep Sea Res., Part A*, *38*, suppl. 1, S531–S571, 1991a.

Davis, R. E., Lagrangian ocean studies, *Annu. Rev. Fluid Mech.*, *23*, 43–64, 1991b.

Figueroa, H. A., and D. B. Olson, Lagrangian statistics in the South Atlantic as derived from SOS and FGGE drifters, *J. Mar. Res.*, *47*, 525–546, 1989.

Flierl, G. R., and J. C. McWilliams, On the sampling requirements for measuring moments of eddy variability, *J. Mar. Res.*, *35*, 797–820, 1977.

Freeland, H. J., P. B. Rhines, and T. Rossby, Statistical observations of the trajectories of neutrally buoyant floats in the North Atlantic, *J. Mar. Res.*, *33*, 383–404, 1975.

Haidvogel, D. B., A. Beckmann, and K. S. Hedström, Dynamical simulations of filament formation and evolution in the coastal transition zone, *J. Geophys. Res.*, *96*, 15,017–15,040, 1991.

Holloway, G., Subgridscale representation, in *Oceanic Circulation Models: Combining Data and Dynamics*, edited by D. T. Anderson and J. Willebrand, pp. 513–593, Kluwer Acad., Norwell, Mass., 1989.

Keffer, T., and G. Holloway, Estimating Southern Ocean eddy flux of heat and salt from satellite altimetry, *Nature*, *332*, 624–626, 1988.

Krauss, W., and C. W. Boning, Lagrangian properties of eddy fields in the northern North Atlantic as deduced from satellite-tracked buoys, *J. Mar. Res.*, *45*, 259–291, 1987.

Lynn, R. J., The subarctic and northern subtropical fronts in the eastern north Pacific Ocean in spring, *J. Phys. Oceanogr.*, *16*, 209–222, 1986.

Mackas, D. L., W. R. Crawford, and P. P. Niiler, A performance comparison for two Lagrangian drifter designs, *Atmos. Ocean*, *27*, 443–456, 1989.

McCreary, J. P., Y. Fukamachi, and P. K. Kundu, A numerical investigation of jets and eddies near an eastern ocean boundary, *J. Geophys. Res.*, *96*, 2515–2534, 1991.

Middleton, J. F., and C. Garrett, A kinematic analysis of polarized eddy fields using drifter data, *J. Geophys. Res.*, *91*, 5094–5102, 1986.

Moffatt, H. K., Transport effects associated with turbulence with particular attention to the influence of helicity, *Rep. Prog. Phys.*, *46*, 621–664, 1983.

Nelson, C. S., Wind stress and wind stress curl over the California Current, *NOAA Tech. Rep., NMFS SSRF-714*, 89 pp., 1977.

Niiler, P. P., R. E. Davis, and H. J. White, Water-following characteristics of a mixed layer drifter, *Deep Sea Res., Part A*, *34*, 1867–1881, 1987.

Niiler, P. P., P.-M. Poulain, and L. R. Haury, Synoptic three-dimensional circulation in an onshore-flowing filament of the California Current, *Deep Sea Res., Part A*, *36*, 385–405, 1989.

Niiler, P. P., A. S. Sybrandy, K. Bi, P. M. Poulain, and D. Bitterman, Measurements of the water following capability of holey-sock and TRISTAR drifters, *Deep Sea Res., Part I*, *42*, 1951–1964, 1995.

Oberhuber, J. M., An atlas based on the 'COADS' data set: The budgets of heat, buoyancy and turbulent kinetic energy at the surface of the global ocean, *Rep. 15*, Max-Planck-Inst. für Meteorol., Hamburg, Germany, 1988.

Paduan, J. D., and P. P. Niiler, A Lagrangian description of motion in northern California coastal transition filaments, *J. Geophys. Res.*, *95*, 18,095–18,110, 1990.

Poulain, P.-M., Near-inertial and diurnal motions in the trajectories of mixed layer drifters, *J. Mar. Res.*, *48*, 793–823, 1990.

Poulain, P.-M., and P. P. Niiler, Statistical analysis of the surface circulation in the California Current system using satellite-tracked drifters, *J. Phys. Oceanogr.*, *19*, 1588–1603, 1989.

Press, W. H., S. A. Teukolshy, W. T. Vetterling, and B. P. Flannery, *Numerical Recipes in FORTRAN: The Art of Scientific Computing*, 2nd ed., 963 pp., Cambridge Univ. Press, New York, 1992.

Reynolds, R. W., and T. M. Smith, A high-resolution global sea surface temperature climatology, *J. Clim.*, *8*, 1571–1583, 1995.

Richardson, P. L., Eddy kinetic energy in the North Atlantic from surface drifters, *J. Geophys. Res.*, *88*, 4355–4367, 1983.

Riser, S. C., and H. T. Rossby, Quasi-Lagrangian structure and variability of the subtropical western North Atlantic circulation, *J. Mar. Res.*, *41*, 127–162, 1983.

Rossby, H. T., S. C. Riser, and A. J. Mariano, The western North Atlantic—A Lagrangian viewpoint, in *Eddies in Marine Science*, edited by A. R. Robinson, pp. 66–91, Springer-Verlag, New York, 1983.

Strub, P. T., et al., The nature of the cold filaments in the California Current system, *J. Geophys. Res.*, *96*, 14,743–14,768, 1991.

Swenson, M. S., P. P. Niiler, K. H. Brink, and M. Abbott, Drifter observations of a cold filament off Point Arena, California, in July 1988, *J. Geophys. Res.*, *97*, 3593–3610, 1992.

Taylor, G. I., Diffusion by continuous movements, *Proc. London Math. Soc.*, *20*, 196–212, 1921.

Venrick, E. L., T. K. Chereskin, T. L. Hayward, A. W. Mantyla, P. P. Niiler, M. D. Ohman, and K. M. Plummer, Physical, chemical and biological data: Cruise Fronts 88, *SIO Ref. 91-7*, 99 pp., Univ. of Calif., San Diego, La Jolla, 1991.

Walsh, J. J., A biological sketchbook for an eastern boundary current, in *The Sea*, vol. 6, edited by E. D. Goldberg, I. N. McCave, J. J. O'Brien, and J. H. Steele, pp. 923–968, Wiley-Interscience, New York, 1977.

Wooster, W. S., and J. L. Reid Jr., Eastern boundary currents, in *The Sea*, vol. 2, edited by M. N. Hill, pp. 253–280, Wiley-Interscience, New York, 1963.

P. P. Niiler, Scripps Institution of Oceanography, University of California, San Diego, 9500 Gilman Drive, La Jolla, CA 92093-0230. (e-mail: niiler@nepac.ucsd.edu)

M. S. Swenson, Atlantic Oceanographic and Meteorological Laboratory, NOAA, 4301 Rickenbacker Causeway, Miami, FL 33149. (e-mail: swenson@aoml.noaa.gov)

(Received November 7, 1995; revised May 7, 1996;
accepted June 6, 1996.)